processes

MDPI

Article

Effects of Calcination Temperature and Calcination Atmosphere on the Performance of Co_3O_4 Catalysts for the Catalytic Oxidation of Toluene

Sicheng Jiang, Zhimin You * and Ning Tang

College of Environment and Resources, Xiangtan University, Xiangtan 411105, China
* Correspondence: youzhm217@163.com; Tel.: +86-15073215836

Abstract: A series of Co_3O_4 catalysts were synthesized and derived from Co-BTC (BTC = 1,3,5-benzenetricarboxylic acid). The effects of different calcination temperatures and calcination atmospheres on the catalytic activity of the materials were investigated. The characteristics of the catalysts were investigated by using various techniques, including X-ray diffraction, N_2 adsorption–desorption measurements, scanning electron microscopy, X-ray photoelectron spectroscopy, and H_2 temperature-programmed reduction. The findings demonstrated that an increase in calcination temperature caused a higher agglomeration of grains, reduced the specific surface area, and influenced the contents of the active substance Co^{3+} and surface-adsorbed oxygen of the catalyst. The catalyst pretreated under the N_2 atmosphere showed a more uniform particle distribution, better low-temperature reducibility, and the highest catalytic activity. The in situ DRIFTS results indicated that toluene was decomposed successively to benzaldehyde, benzoic acid, bicarbonate, and carbonate species and was eventually broken down into small molecules of CO_2 and H_2O as the temperature increased.

Keywords: Co_3O_4; catalysts; toluene; catalytic activity

check for updates

Citation: Jiang, S.; You, Z.; Tang, N. Effects of Calcination Temperature and Calcination Atmosphere on the Performance of Co_3O_4 Catalysts for the Catalytic Oxidation of Toluene. *Processes* **2023**, *11*, 2087. https://doi.org/10.3390/pr11072087

Academic Editors: Miguel Ladero Galán, Lingling Ma, Yang Shao and Min Luo

Received: 24 February 2023
Revised: 18 May 2023
Accepted: 16 June 2023
Published: 13 July 2023

Copyright: © 2023 by the authors. Licensee MDPI, Basel, Switzerland. This article is an open access article distributed under the terms and conditions of the Creative Commons Attribution (CC BY) license (https://creativecommons.org/licenses/by/4.0/).

1. Introduction

Volatile organic compounds (VOCs) are generally defined as the sum of a range of carbon-based organic air pollutants with boiling points ranging from 50 to 260 °C and a Reid vapor pressure greater than 10.3 Pa at a normal temperature (293.15 K) and pressure (101.325 kPa) [1,2]. VOCs have the characteristics of easy volatility, easy diffusion, and easy poisoning and have become major pollutants in the atmosphere [3,4]. Toluene is usually considered to be one of the most typical representatives of VOCs, with a wide range of sources and easy poisoning characteristics in various types of air pollution, such as ozone pollution, fine particulate matter pollution, and secondary aerosol pollution, and it is often an important precursor of direct or indirect harm to the environment and human body, causing widespread concern in society [5,6]. Among the reported methods for toluene removal, catalytic oxidation is considered to be one of the most effective and economical ways to remove toluene, due to its low energy consumption, fast reaction rate, high feasibility, and lack of secondary pollution [7,8].

The choice of catalyst in catalytic oxidation plays a key role in the degradation efficiency of VOCs. The metal catalysts currently used for the degradation of toluene can be divided into noble metal catalysts and non-noble metal oxide catalysts [9,10]. Although noble metal catalysts exhibit outstanding performance for the catalytic removal of VOCs at low temperatures, their susceptible poisoning and high costs have limited their widespread application. Therefore, transition metal oxides have been considered as an alternative for the oxidation of VOCs, due to their relatively low cost, superior reducibility, and anti-poisoning ability [11,12]. Among the non-noble metal oxide catalysts, Co_3O_4 has the advantages of low cost and being environmentally friendly [13,14]. In related studies, Co_3O_4 catalysts showed excellent catalytic activity in the degradation process of toluene,

and the high activity of Co_3O_4 catalysts is related to the presence of mobile oxygen in their spinel-type structures, which gives them good low-temperature reduction ability and a large number of oxygen vacancies and adsorbed oxygen content on the surface [15,16]. However, the specific surface area, pore structure, and physical and chemical properties of Co_3O_4 catalysts also play an important role in the degradation of toluene [17]. Therefore, most of the research is devoted to the synthesis of Co_3O_4 catalysts with different structures by different preparation methods [13,17]; however, traditional methods are not conducive to controlling the particle size and structure within the catalyst [18]. Therefore, a simple and controllable method is needed to prepare Co_3O_4 catalysts to achieve high-efficiency degradation of toluene.

In recent years, metal–organic frameworks (MOFs) have attracted widespread interest due to their large specific surface areas, flexible and tunable structures, and versatile properties [19,20]. The nature of the MOFs—namely, that their highly ordered metal nodes are well separated by long chains of organic ligands [21]—also allows the nanometal oxides prepared by direct pyrolysis of MOFs to have highly dispersed metal active centers while still retaining their original pore structure [20]. This provides a very effective method for the design of Co_3O_4 catalysts. It has been demonstrated that Co_3O_4 catalysts derived from Co-MOFs showed good degradation of toluene. Juan Lei and his co-workers synthesized Co_3O_4 catalysts with octahedral, dodecahedral, and rod shapes using three different Co-MOFs; among them, the ZSA-1-Co_3O_4 catalyst with an octahedral shape showed the best toluene degradation activity, with 90% toluene conversion reached at 249 °C using a gaseous hourly space velocity (GHSV) of 40,000 $mL \cdot g^{-1} \cdot h^{-1}$ for 1000 ppm of toluene [22].

However, the monometallic catalysts derived from MOFs are generally vulnerable to clustering or sintering during pyrolysis, which leads to larger metallic particles and poorer dispersion, resulting in the reduced catalytic activity of the catalyst [23]. Juan Lei and his colleagues investigated the effects of different calcination temperatures on the catalytic activity of Co_3O_4 catalysts and found that the catalysts exhibited different physical and chemical properties under different calcination temperatures, with Co_3O_4 prepared at 350 °C having the largest specific surface area and pore volume and the highest Co^{3+}/Co^{2+} and O_{ads}/O_{latt} values, meaning the highest catalytic activity in the catalytic degradation of toluene [24]. Xiaodong Zhang and his co-workers prepared Mn_2O_3 catalysts in different pyrolysis atmospheres and found that the catalytic activity of the Mn_2O_3 catalyst pretreated with Ar and then with O_2 had the highest Mn^{3+} and adsorbed oxygen content, and its catalytic activity was superior to that of the Mn_2O_3 catalysts treated with either Ar or O_2 alone [25]. However, most of the existing studies have been limited to investigating the effects of the calcination temperature on the catalysts or the effects of the calcination atmosphere on the catalysts; the synergistic influences of the calcination temperature and atmosphere on the physical and chemical properties of materials have not been comprehensively analyzed.

Herein, we provide a simple method using Co-MOFs as a precursor to obtain honeycomb–spherical structures and Co_3O_4 catalysts for the degradation of toluene. In order to determine the influence mechanism of the Co_3O_4 catalysts formed by the calcination temperature and calcination atmosphere on the degradation activity of toluene, the ideal synthetic route for the synthesis of Co_3O_4 materials using Co-BTC as a precursor was explored to provide a reference for the synthesis process of metal oxides derived from MOFs. Finally, the catalyst was subjected to in situ IR tests under different atmospheric conditions to explore the toluene degradation process and intermediate products.

2. Experimental Section

2.1. Preparation of Catalysts

2.1.1. Synthesis of Co-BTC

Co-BTC was synthesized by a simple solvothermal method. Typically, 0.01 mol of BTC was added to 120 mL of a mixture of DMF, ethanol, and water, with a volume ratio of 8:1:1. After the mixture was completely dissolved, 0.012 mol of $Co(NO_3)_2 \cdot 6H_2O$ was added

to the mixed solution and stirred for 30 min with a magnetic stirrer. Then, the resulting solution was poured into a 200 mL Teflon-lined autoclave and heated at 150 °C for 24 h. After cooling naturally to room temperature, the product was separated using sand core filters. The collected precipitate was added to 30 mL of ethanol and stirred using a magnetic stirrer for 30 min to remove the unreacted chemicals from the material, before being filtered by repeated rinsing with ethanol. The obtained product was dried at 80 °C overnight to obtain the Co-BTC material.

2.1.2. Synthesis of Co_3O_4 Catalysts

Co-BTC was calcined in air at different temperatures (350 °C, 450 °C, and 550 °C) for 2 h at a heating rate of 2 °C·min^{-1}; the products were named Co_3O_4-350, Co_3O_4-450, and Co_3O_4-550, respectively. Then, the Co-BTC was calcined at 450 °C in N_2 for 2 h at a heating rate of 2 °C·min^{-1} to obtain Co_3O_4-N_2. Additionally, the sample of Co-BTC was first treated at 450 °C in N_2 for 1 h and then treated at 350 °C in O_2 for 1 h, and the product was named Co_3O_4-N_2-O_2. As a comparison, 0.012 mol of the $Co(NO_3)_2 \cdot 6H_2O$ was treated at 450 °C in N_2 for 1 h and then treated at 350 °C in air for 1 h to obtain Co_3O_4-P.

2.2. Characterization of Materials

The thermal stability of Co-BTC was tested via thermogravimetric analysis (TGA) using an STA-449 F4 Jupiter thermal analyzer (Netzsch, Germany). The weight change in the catalyst was recorded from room temperature to 750 °C under different air and N_2 conditions, at a heating rate of 2 °C·min^{-1}. Powder X-ray diffraction (XRD) patterns were recorded on a Bruker D8 Advance powder diffraction system using Cu-Kα radiation in a 2θ range of 5–90°, at a scanning rate of 5°·min^{-1}. The catalysts' specific surface areas, pore volumes, and pore size distribution were determine using a Micromeritics ASAP 2460 Automated Gas Sorption analyzer. Surface areas were determined using the Brunauer−Emmett−Teller (BET) method; pore volumes and pore size distribution were determined using the Barrett−Joyner−Halenda (BJH) method. A ZEISS Sigma 300 scanning electron microscope (SEM) (Oberkochen, Germany) was operated at an accelerating voltage of 15 kV. The catalyst was deposited on a clean silicon wafer, mounted on the aluminum holder using carbon tape, and sputter-coated with gold to minimize sample charging. X-ray photoelectron spectroscopy (XPS) analysis was performed using a Thermo Fisher Scientific spectrophotometer with Al Kα (1486.6 eV) as an X-ray excitation source. Survey scans and narrow scans were carried out at pass energies of 100 eV and 30 eV, respectively. C1 s was used as a reference and assigned a binding energy of 284.8 eV. The Micromeritics AutoChem II 2920 chemical adsorption apparatus was used for a hydrogen temperature-programmed reduction (H_2-TPR) experiment. Before the H_2-TPR experiment, 0.1 g of catalyst was pretreated under an Ar atmosphere at 150 °C for 1 h. The temperature was then cooled to 50 °C and the reduction process began, proceeding in a temperature range of 50–800 °C in 10% vol. H_2/Ar (30 mL·min^{-1}). In situ diffusion reflectance infrared Fourier-transform spectrophotometry (DRIFTS; Nicolet is 50) was employed to investigate the reaction process of toluene oxidation over Co_3O_4-N_2-O_2. The catalyst was squeezed into a thin slice in the DRIFT cell and tested in situ using absorbance; it was then activated to remove surface impurities under Ar for 1 h at 200 °C, and then cooled to room temperature. Toluene (200 ppm) was introduced until the peaks remained unchanged. Subsequently, Ar or air was used to record changes in IR peaks at different temperatures under different gas atmospheres.

2.3. Catalytic Testing

The catalytic oxidation of toluene was carried out in a fixed-bed flow reactor at atmospheric pressure. First, 100 mg of catalyst was packed into a quartz tube 10 cm in length, with an inner diameter of 2 cm; the ends were held in place by quartz fiber, and the reaction temperature was controlled using a tubular furnace (KTF-0.5-06). Toluene was injected from a single-channel syringe pump (SPLab01) into the gasification chamber, and

the gasified toluene was carried through 100 mL·min^{-1} air into a quartz tube (the gas flow was controlled using a gas flowmeter). For toluene, the reacted gas was detected using gas chromatography (GC112A), and the detection conditions were as follows: high-purity N_2 was used as a carrier gas; a flame ionization detector (FID) was used; the column temperature was 150 °C; the gasification chamber temperature was 250 °C; the detector temperature was 250 °C; and the chromatographic column was a capillary column. For CO_2, the reacted gas was detected using a multifunctional gas analyzer (GT-2000). Toluene's conversion (η) and mineralization (μ) were calculated according to the following equations:

$$\eta = \frac{C_0 - C_i}{C_0} \times 100\%$$

$$\mu = \frac{C_{CO_2,out}}{C_{CO_2,in}} \times 100\%$$

where C_0 (ppm) and C_i (ppm) are the toluene concentrations of the inlet and outlet gases, respectively, while $C_{CO_2,in}$ (ppm) and $C_{CO_2,out}$ (ppm) represent the concentration of carbon dioxide at the time of complete oxidation of toluene and the concentration of carbon dioxide at the outlet after the reaction, respectively.

Reaction rates over catalysts and apparent activation energies (E_a) were calculated for toluene conversions lower than 20%, in line with the practice previously described in the literature [24].

3. Results and Discussion

3.1. Structural Analysis

The XRD patterns of all catalysts are presented in Figure 1. It can be seen that the air-calcined Co_3O_4 catalysts in the 2θ range of 5–90° displayed similar patterns, which corresponded to the standard Co_3O_4 sample (Co_3O_4-PDF#74-2120). The characteristic diffraction peaks of Co_3O_4 at 19°, 31.3°, 36.8°, 44.8°, 59.4°, and 65.2° corresponded to the (111), (220), (311), (400), (511), and (440) crystal faces, respectively. This showed that the air-calcined Co-BTC ended up with a Co_3O_4 crystal-phase structure. The Co_3O_4-N_2 nanomaterial exhibited faint diffraction peaks at 2θ of 36.6°, 42.6°, and 61.8°, which corresponded to the (111), (200), and (220) lattice planes, respectively, of pure CoO (CoO-PDF#75-0533). It was found that the Co in the Co_3O_4-N_2 catalyst existed mainly in the form of CoO, due to the fact that, in the absence of oxygen, Co mainly combines with oxygen bonds to form CoO. From Figure 1 and Tables S1 and S2, it can clearly be seen that the peak intensity of Co_3O_4 was enhanced and its width narrowed with increasing air calcination temperature, indicating that with the increase in calcination temperature, O_2 oxidized the metal clusters in the Co-BTC skeleton more fully, resulting in better crystallization of Co_3O_4 and the formation of metal oxide clusters with larger particles. By comparing the diffraction peaks of the metal oxides formed in different calcination atmospheres, it was found that the oxides calcined with N_2 had lower peak intensities and larger peak widths, especially for the Co_3O_4-N_2 catalyst, indicating that the Co_3O_4-N_2 catalyst had a smaller particle size.

The N_2 adsorption−desorption isotherms and BJH pore size distributions of the Co_3O_4 catalysts are shown in Figure S2. The catalysts all exhibited type IV isotherms with H3-type hysteresis loops, indicating that the catalysts had similar mesoporous structures [26,27]. Table 1 shows the specific surface area, average pore size, and pore volume data for the different catalysts. It can be seen that the influence of the calcination temperature on the pore structure of the material was significant. With the increase in temperature, the specific surface area, average pore size, and pore volume of the material all decreased as a result of agglomeration and expansion between crystals at high calcination temperatures (Figure 2). In addition, the calcination atmosphere also affected the pore structure of the material. It was found that the oxides calcined under an N_2 atmosphere had a larger specific surface area. Co_3O_4-N_2 had the largest specific surface area (161.4 m^2·g^{-1}), and this was attributed to the carbonization of the organic ligands in Co-BTC under the N_2 atmosphere, which

enabled the material to maintain its original skeletal structure. It was also found that Co_3O_4-N_2-O_2 had the largest average pore size, which facilitated the transfer process between reactants and products.

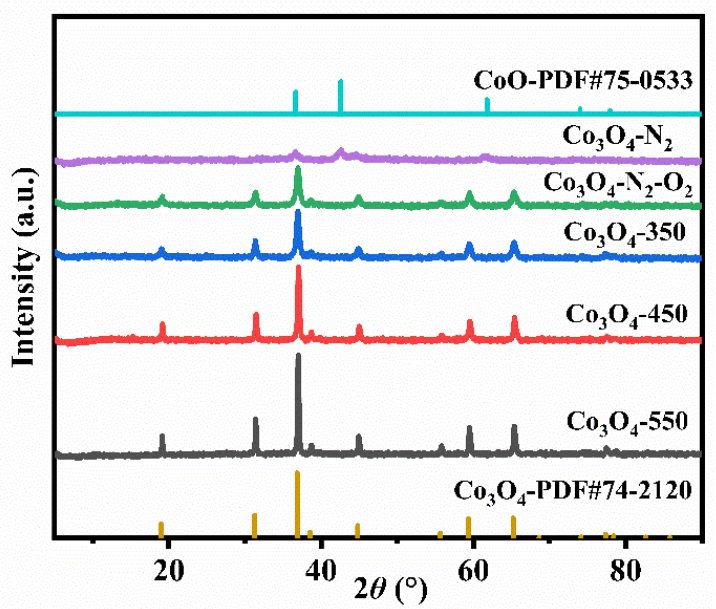

Figure 1. XRD patterns of Co_3O_4 catalysts.

Table 1. Specific surface area and pore structure data of Co_3O_4 catalysts.

Samples	BET Surface Area ($m^2 \cdot g^{-1}$)	Average Pore Size (nm)	Pore Volume ($cm^3 \cdot g^{-1}$)
Co_3O_4-550	8.7	4.9	0.01
Co_3O_4-450	16.8	9.4	0.04
Co_3O_4-350	40.2	17.9	0.18
Co_3O_4-N_2-O_2	57.2	21.25	0.3
Co_3O_4-N_2	161.4	11.51	0.46

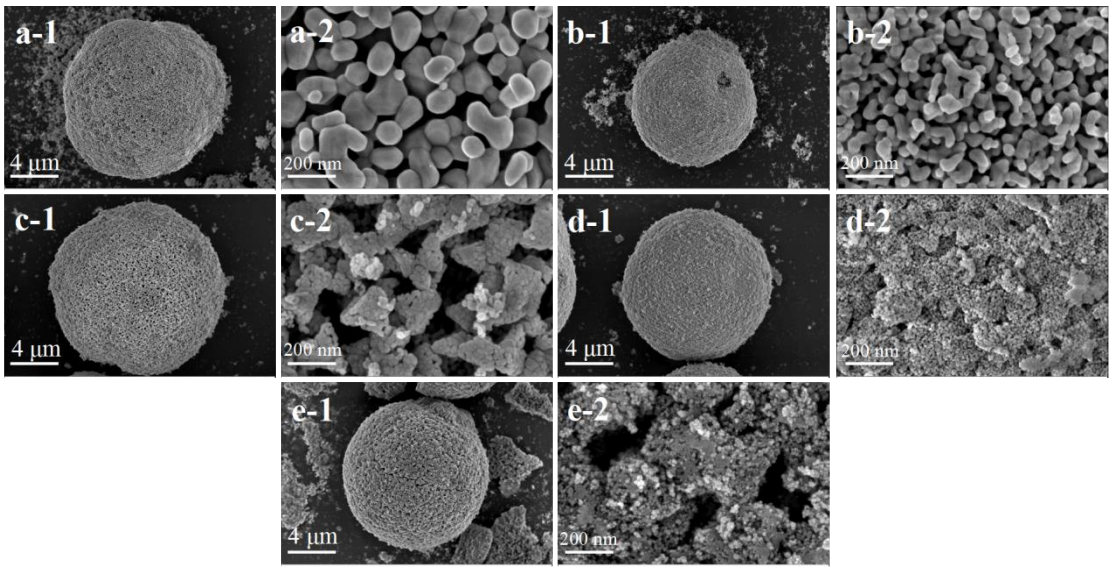

Figure 2. SEM images with different magnification (4 μm and 200 nm) of (**a-1**,**a-2**) Co_3O_4-550, (**b-1**,**b-2**) Co_3O_4-450, (**c-1**,**c-2**) Co_3O_4-350, (**d-1**,**d-2**) Co_3O_4-N_2-O_2, and (**e-1**,**e-2**) Co_3O_4-N_2.

The microstructures of the catalysts are presented in Figure 2. It can be seen that all catalysts exhibited a honeycomb-like spherical structure. From Figure 2a–c, it can also be seen that the pore structure inside the Co_3O_4-350 catalyst spheres was composed of a number of aggregated grains. As the air calcination temperature was increased, the surface of these grains gradually became smooth, and the particle size also showed signs of expansion, indicating that sintering and agglomeration between the grains occurred at high temperatures, resulting in a decreasing specific surface area of the catalyst, which was consistent with the results of the XRD and BET characterizations. The Co_3O_4-N_2-O_2 catalyst spheres showed no obvious aggregation between the grains and exhibited a highly discrete and uniform distribution; this indicated that the catalyst exhibited more roughness and possessed a larger specific surface area, facilitating the exposure of the Co active sites in the catalyst, and thereby increasing the chance of contact with toluene and improving the catalytic oxidation activity of the catalysts.

3.2. Surface Composition and Reduction Behavior

To obtain further information about elemental chemical states and surface oxygen species, the Co $2p_{3/2}$ and O 1s XPS spectra of the samples were obtained, as shown in Figure 3a,b, respectively. The Co $2p_{3/2}$ XPS peak could be fitted to two component peaks and two satellite peaks, with the main peaks at binding energies of 779.5 eV and 781.29 eV corresponding to the Co^{3+} and Co^{2+} species, and the main peaks at binding energies of 785.68 eV and 789.02 eV corresponding to the Co^{3+} and Co^{2+} satellite peaks [28,29]. The Co^{3+} and Co^{2+} contents and the corresponding Co^{3+}/Co^{2+} ratios were calculated from the peak areas, and the data are presented in Tables 2 and 3. The ratio of Co^{3+}/Co^{2+} increased in the order of Co_3O_4-N_2 < Co_3O_4-550 < Co_3O_4-450 < Co_3O_4-350 ≈ Co_3O_4-N_2-O_2, where Co_3O_4-350 and Co_3O_4-N_2-O_2 exhibited the highest values of Co^{3+}/Co^{2+}, indicating the presence of abundant Co^{3+} species in Co_3O_4-350 and Co_3O_4-N_2-O_2. Previous studies have shown that Co^{3+} usually acts as the active center of toluene and can effectively promote the degradation of toluene [30].

Figure 3b shows the O 1s XPS spectra of the samples, which could be divided into two peaks at binding energies of 529.36 eV and 531.03 eV, respectively. This could be ascribed to lattice oxygen (O_{latt}) and adsorbed oxygen species on oxygen vacancies (O_{ads}) [31], where the Co_3O_4-N_2 catalyst shifted the position of the oxygen species peak, so that the peaks with binding energies at 529.66 eV and 531.54 eV represented lattice oxygen species and adsorption oxygen, respectively. The O_{ads}/O_{latt} molar ratios were determined based on the area-fitted curve peaks of the O 1s XPS spectra; these are listed in Tables 2 and 3. It can be seen that the ratio of O_{ads}/O_{latt} decreased as the calcination temperature of the material increased, indicating that high-temperature calcination was not conducive to the accumulation of adsorbed oxygen in the material. Previous studies have shown that surface-adsorbed oxygen (O_{ads}) is related to surface defects and that higher contents of O_{ads} facilitate the uptake and activation of gas-phase oxygen molecules by the catalyst, promoting the degradation of pollutants [32,33]. In addition, it is worth noting that Co_3O_4-N_2 had the highest O_{ads}/O_{latt} molar ratios. However, from Figure S3 and Table 3, it can also be seen that the surface C, O, and Co contents of the Co_3O_4-350 and Co_3O_4-N_2-O_2 catalysts were essentially the same, with the highest elemental content being that of O, accounting for about 50% of the total. In contrast, the Co_3O_4-N_2 catalyst had the largest amount of elemental C but only 23% of the total amount of O. This was because the Co_3O_4-N_2 catalyst was prepared in the absence of oxygen, so most of the organic matter in the ligand was stored as carbon inside the catalyst, and the metal Co inside the material could not be fully oxidized, resulting in a lack of sufficient O in the catalyst itself, so that the Co_3O_4-N_2 catalyst had the highest O_{ads}/O_{latt} molar ratios but the lowest total amount of O_{ads} compared with other catalysts. This phenomenon can also be seen in Figure S1.

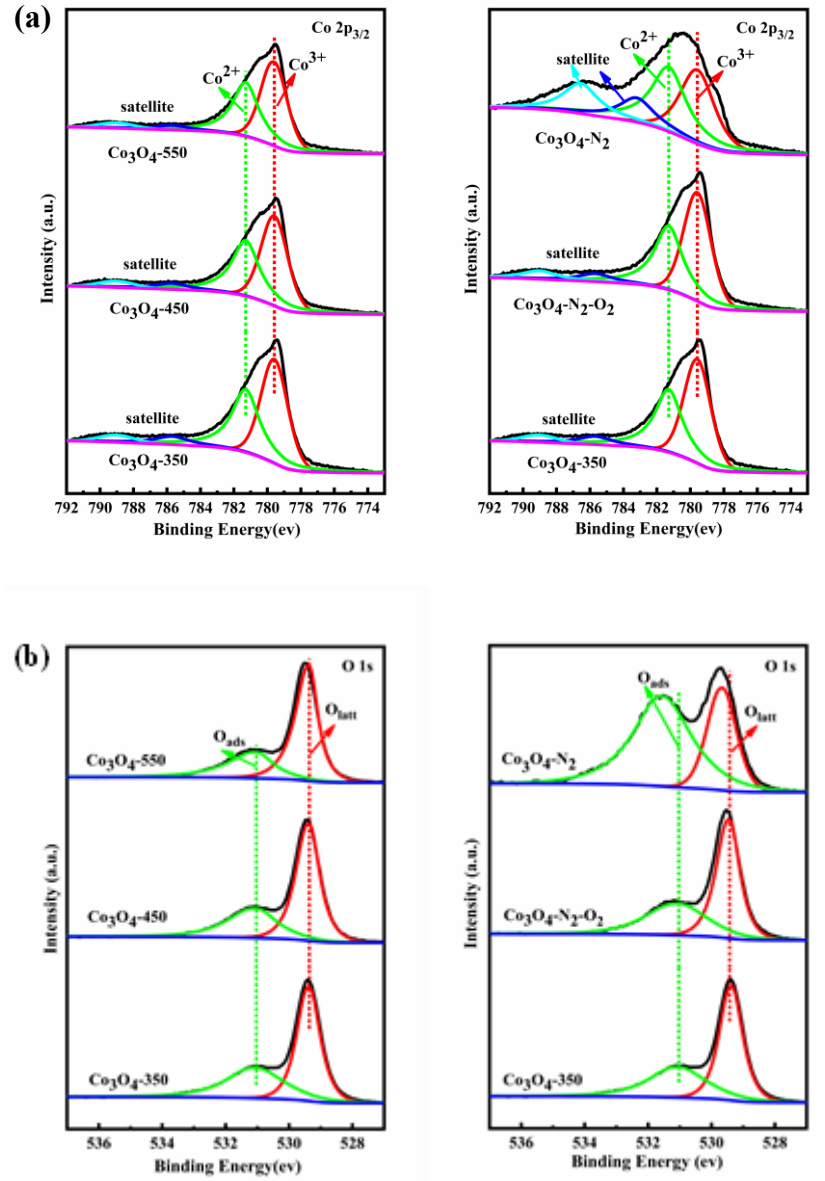

Figure 3. XPS spectra of Co_3O_4 catalysts: (**a**) Co $2p_{3/2}$; (**b**) O 1s.

Table 2. XPS surface element analysis of catalysts prepared at different calcination temperatures.

Samples	Co^{3+}(%)	Co^{2+}(%)	Co^{3+}/Co^{2+}	O_{ads}(%)	O_{latt}(%)	O_{ads}/O_{latt}
Co_3O_4-350	53.29	46.71	1.14	41.46	58.54	0.70
Co_3O_4-450	51.69	48.31	1.06	36.43	63.57	0.57
Co_3O_4-550	50.28	49.72	1.01	33.06	66.94	0.49

Table 3. XPS surface element analysis of catalysts prepared with different atmospheres.

Samples	C(%)	O(%)	Co(%)	Co^{3+}/Co^{2+}	O_{ads}/O_{latt}
Co_3O_4-350	29.90	47.34	22.75	1.14	0.70
Co_3O_4-N_2-O_2	27.55	50.04	22.40	1.18	0.74
Co_3O_4-N_2	64.02	23.06	12.92	0.96	1.92

The reducibility of a sample was highly related to its catalytic performance. Figure 4 illustrates the H_2-TPR profiles of all synthesized catalysts. Three distinct reduction peaks

were found for all catalysts, in which the low-temperature-region reduction peak indicated the reduction of Co^{3+} to Co^{2+}, the medium-temperature-region reduction peak indicated the reduction of Co^{2+} to Co^{+}, and the high-temperature-region reduction peak indicated the reduction of Co^{2+} to Co^{0} [34]. From Figure 4a, it can be seen that the reduction peak of the catalyst gradually moved towards the high-temperature region as the calcination temperature increased, indicating that the reduction effect of the material deteriorated under high-temperature calcination conditions; this may be related to the particle size of the catalyst, as the XRD results indicated that the particle size of the catalyst became larger as the calcination temperature increased. It has been reported in the literature that the reduction peak tends to move towards the high-temperature region as the particle size increases [35]. Figure 4b shows the reduction peaks of the catalysts prepared in different calcination atmospheres. A comparison reveals that Co_3O_4-N-O_2 had the lowest reduction temperature. This finding may be related to the specific surface area of the material and the abundance of Co^{3+} active centers, i.e., the high specific surface area of the material made it easier to expose a large number of Co^{3+} active sites on the external surface. Compared with Co_3O_4-N_2-O_2, the reduction peak of Co_3O_4-N_2 was very weak, because the Co in the Co_3O_4-N_2 catalyst existed mainly in the form of CoO and, thus, lacked a sufficient number of Co^{3+} active sites.

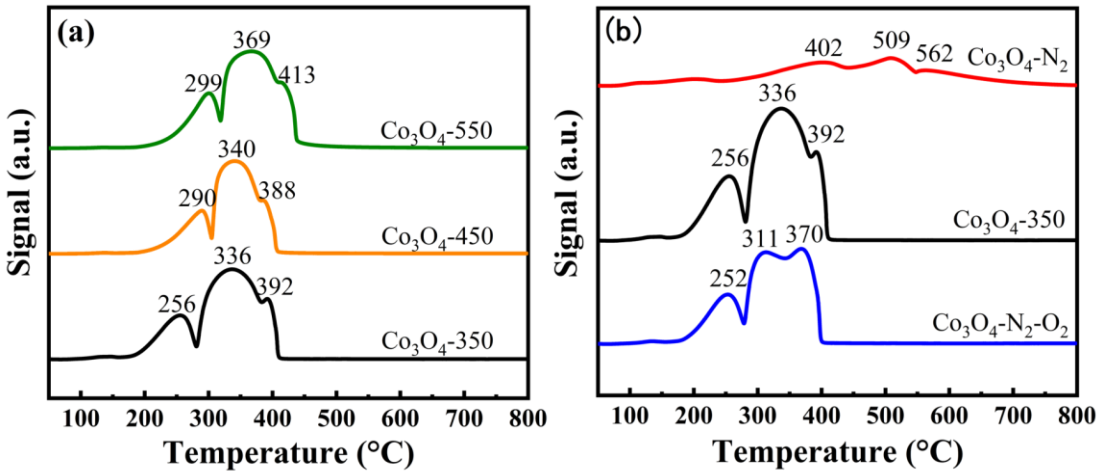

Figure 4. H_2-TPR spectra of Co_3O_4 catalysts under (**a**) different calcination temperatures and (**b**) different calcination atmospheres.

3.3. Catalytic Performance

Figure 5a,b show the temperature dependence of the catalytic efficiency in toluene conversion for all as-prepared catalysts under the conditions of toluene concentration = 1000 ppm and WHSV = 60,000 $mL \cdot g^{-1} \cdot h^{-1}$. It can be seen from the graph that no catalyst showed any significant toluene degradation below 210 °C; subsequently, as the temperature increased, the catalysts' active sites were gradually activated and the toluene degradation rate rapidly increased. From Figure 5a, it can be seen that increasing the calcination temperature of the catalyst did not promote catalytic activity, because this increase in calcination temperature also caused the particle size of the catalyst to gradually increase, resulting in a decreased specific surface area of the catalyst, which was not conducive to the exposure of the active sites. From Figure 5b, it can be seen that the different calcination atmospheres of the materials also had an effect on the degradation of toluene. The Co_3O_4-N_2-O_2 catalyst exhibited the best catalytic effect, while the Co_3O_4-N_2 catalyst had the poorest, i.e., the worst degradation of toluene. This was because the catalytic activity of the catalyst was not only related to the specific surface area of the material—the Co^{3+} active sites and surface-adsorbed oxygen content were also important influencing factors. The degradation activity of the catalyst for toluene decreased as follows: Co_3O_4-N_2-O_2 > Co_3O_4-350 > Co_3O_4-450 > Co_3O_4-N_2 > Co_3O_4-550. The best toluene degradation rates were produced by

Co_3O_4-N_2-O_2. The T_{10}, T_{50}, and T_{90} temperatures required for 10%, 50%, and 90% toluene conversion were 221 °C, 234 °C, and 245 °C, respectively. In combination with the above characterization, these findings demonstrate that the catalytic activity of the catalysts was determined by a combination of the specific surface area, the morphology, the contents of Co^{3+} active sites and surface-adsorbed oxygen, and the redox properties of the material. In short, we found that a large specific surface area, homogeneous grain distribution, high Co^{3+} and surface-adsorbed oxygen contents, and excellent redox properties promoted the catalytic activity of the material.

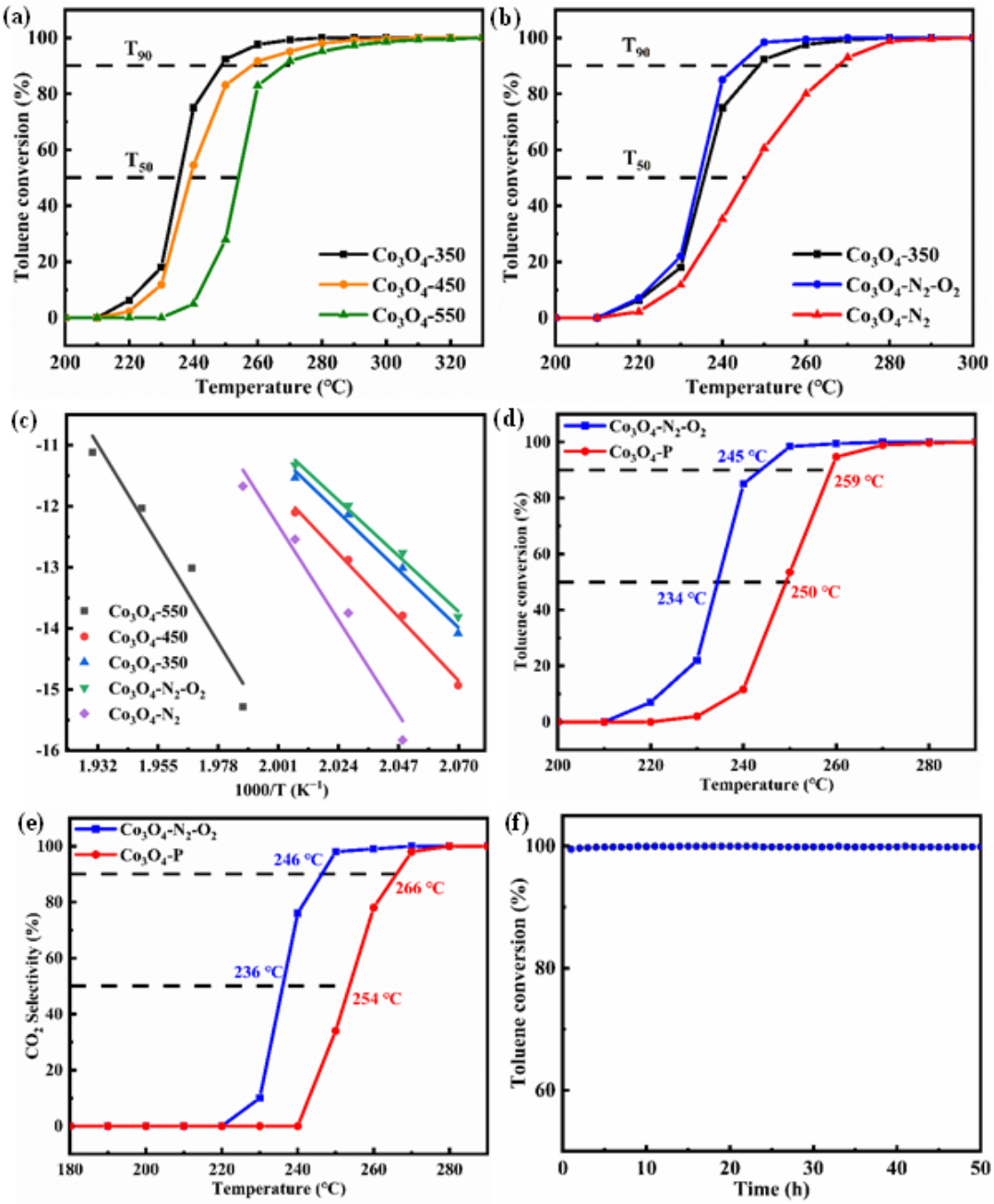

Figure 5. Toluene degradation rates of Co_3O_4 catalysts under (**a**) different calcination temperatures; and (**b**) different calcination atmospheres (0.1 g catalyst; 1000 ppm toluene; WHSV = 60,000 $mL \cdot g^{-1} \cdot h^{-1}$); (**c**) Arrhenius plots; (**d**,**e**) comparison of (**d**) toluene catalytic performance and (**e**) CO_2 selectivity of Co_3O_4-N_2-O_2 and Co_3O_4-P (0.1 g catalyst; 1000 ppm toluene; WHSV = 60,000 $mL \cdot g^{-1} \cdot h^{-1}$); (**f**) Co_3O_4-N_2-O_2 on-stream stability test of continuous catalytic process (0.1 g catalyst; 1000 ppm toluene; WHSV = 60,000 $mL \cdot g^{-1} \cdot h^{-1}$; T = 260 °C).

The apparent activation energy (Ea) of the catalysts was calculated by applying the linear fitting of Arrhenius plots at a conversion rate of less than 20% (as shown in Figure 5c). The calculated results are listed in Table S3 in the following order: Co_3O_4-N_2-O_2 (39.65 kJ·mol^{-1}) < Co_3O_4-350 (42.06 kJ·mol^{-1}) < Co_3O_4-450 (47.84 kJ·mol^{-1}) < Co_3O_4-N_2 (67.27 kJ·mol^{-1}) < Co_3O_4-550 (70.43 kJ·mol^{-1}). The lowest Ea value corresponds to the highest possibility of toluene decomposition. These results were consistent with those of toluene conversion.

In order to explore the advantages of Co_3O_4 catalysts derived from Co-MOF in terms of catalytic activity and mineralization rate, we carried out a test in which Co_3O_4-N_2-O_2 (with the best catalytic activity) was used as the catalyst. The toluene conversion rates and CO_2 yields were measured for both the Co_3O_4-N_2-O_2 and Co_3O_4-P catalysts. As can be seen in Figure 5d,e, we found that the Co_3O_4-N_2-O_2 catalyst achieved obviously higher conversion rates at lower temperatures than the Co_3O_4-P catalyst, in terms of both toluene degradation efficiency and mineralization efficiency. The toluene degradation efficiencies of Co_3O_4-N_2-O_2 catalysts at 50% and 90% were 234 °C and 245 °C, respectively, and these values were broadly consistent with the temperatures corresponding to toluene mineralization efficiencies at 50% and 90% (236 °C and 246 °C, respectively). This showed that the Co_3O_4-N_2-O_2 catalyst could adequately convert toluene molecules to CO_2 and H_2O at the appropriate temperature, thereby reducing the emission of intermediate products during the reaction.

Figure 5f shows results of a continuous test of the catalytic oxidation of toluene over the Co_3O_4-N_2-O_2 catalyst. The test results demonstrated that the toluene degradation efficiency of the catalyst remained above 99% for 50 h at 260 °C, without any significant decline, indicating that the catalytic activity of the Co_3O_4-N_2-O_2 catalyst does not change over time and exhibits good catalytic stability when operated for a long period at an appropriate temperature, suggesting great potential for its usage in practical applications.

3.4. Mechanism for Degradation of Toluene over Co_3O_4-N_2-O_2

To further investigate the possible reaction pathway of toluene oxidation on the Co_3O_4-N_2-O_2 catalyst and any intermediates in the degradation of toluene, in situ DRIFT spectra of the catalyst at different temperatures under Ar and air conditions were obtained, as shown in Figure 6. It was found that, after a period of introducing toluene at room temperature, characteristic peaks of toluene appeared: at 3091 and 3035 cm^{-1}, attributed to unsaturated C-H bonds on the benzene ring; and at 2932 cm^{-1}, attributed to saturated C-H bonds on toluene's methyl groups. In addition. 1585 and 1495 cm^{-1} were found to be the benzene ring skeleton vibration peaks of toluene [36–38], indicating that toluene was adsorbed on the surface of the catalyst. Figure 6a shows that the characteristic peak of toluene did not change significantly with increasing temperature under an Ar atmosphere, meaning that the catalyst had little degradation effect on toluene under an Ar atmosphere. Conversely, under air-supply conditions, as shown in Figure 6b, the characteristic peak of toluene disappeared with the increase in temperature. At 140 °C, new bands appeared at 2840 and 2721 cm^{-1}, which could possibly be attributed to adsorbed benzaldehyde [39]; in addition, bicarbonate species (1356 cm^{-1}) also started to appear [40]. New characteristic peaks also appeared at 1563 and 1340 cm^{-1} when the temperature reached 200 °C; these were attributed to benzoic acid and carbonate species, respectively [41,42]. As the temperature increased, benzaldehyde was further oxidized to benzoic acid, and bicarbonate species were gradually oxidized to carbonate species. The characteristic peaks of 1431 cm^{-1} for carboxylate species such as benzoic acid, and of 2340 and 2360 cm^{-1} for CO_2, became progressively larger as the temperature increased under an air atmosphere [38], meaning that more and more benzoic acid and CO_2 were generated and accumulated on the catalyst's surface as the temperature increased.

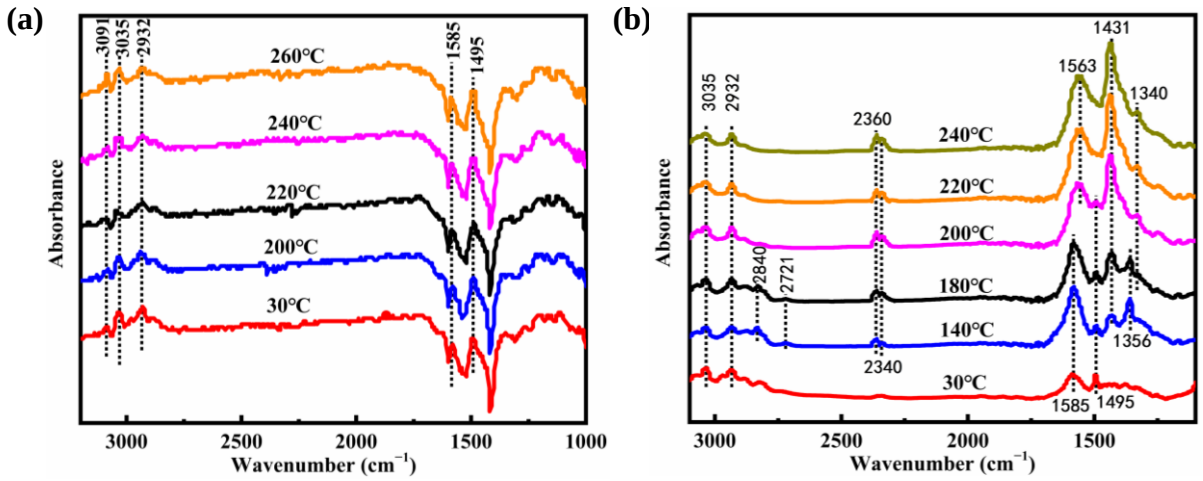

Figure 6. In situ DRIFT spectra of toluene oxidation of Co_3O_4-N_2-O_2 in Ar (**a**) and air (**b**).

The above analysis clearly demonstrates that the toluene molecules in the air were adsorbed on the surface of the catalyst, and that the catalytic oxidation effect of the lattice oxygen of the catalyst on toluene adsorbed on the catalyst's surface was not significant. The degradation process of toluene molecules is shown in Figure 7. The toluene molecules were first adsorbed on the catalyst's surface and then gradually degraded by the interaction with the adsorbed oxygen. With increasing temperature, the toluene molecules were gradually oxidized into benzaldehyde, benzoic acid, and bicarbonate and carbonate species, and finally decomposed into small molecules of CO_2 and H_2O [42].

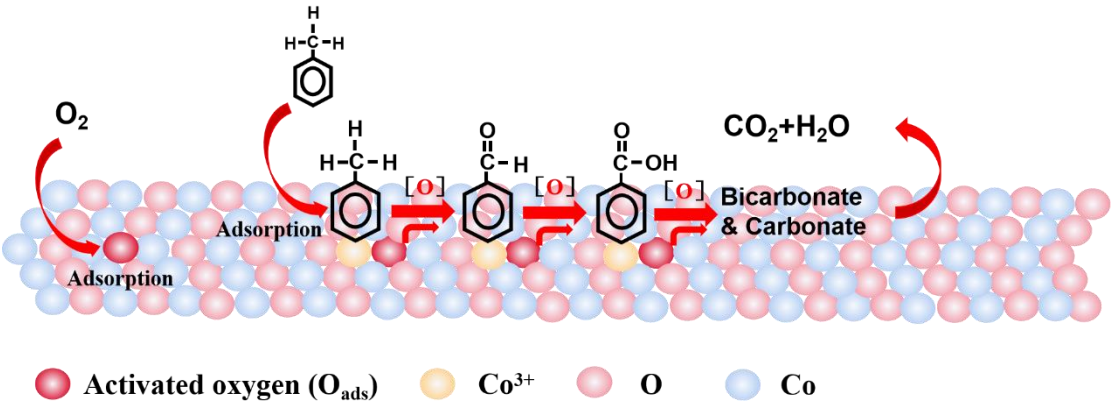

Figure 7. Degradation process of toluene by Co_3O_4-N_2-O_2 catalyst.

4. Conclusions

Different Co_3O_4 catalysts were prepared under different calcination temperatures and calcination atmospheres, and their degradation effects on toluene were compared. It was found that increasing the air calcination temperature intensified the agglomeration of the internal grains of the catalyst and reduced the contents of Co^{3+} active sites and surface-adsorbed oxygen; this was not conducive to the improvement of the catalytic activity of the material. However, pretreatment with N_2 significantly improved the internal structure of the catalyst, making the internal grains of the catalyst more uniformly distributed; this promoted the exposure of active sites and improved the degradation efficiency of toluene. The Co_3O_4-N_2-O_2 catalyst exhibited superior toluene degradation activity and better toluene mineralization rates compared with Co_3O_4-P; it also exhibited stable catalytic activity, indicating its great potential for practical applications. Finally, the degradation process of toluene on the surface of Co_3O_4-N_2-O_2 catalyst was investigated; it was found that benzaldehyde, benzoic acid, and bicarbonate and carbonate species are intermediate

products in the degradation process of toluene, which are ultimately decomposed into small molecules of CO_2 and H_2O with increased temperature.

Supplementary Materials: The following supporting information can be downloaded at: https://www.mdpi.com/article/10.3390/pr11072087/s1. Figure S1: Thermal weight curve of Co-BTC; Figure S2: N_2 adsorption and desorption isotherms of samples (**a**) different calcination atmosphere and (**b**) calcination temperature in air, and (**c**) pore-size distributions of all samples. Figure S3: XPS full spectra of Co_3O_4 catalysts. Table S1: Peak height of the XRD diffraction peaks of the catalysts. Table S2: FWHM of the XRD diffraction peaks of the catalysts. Table S3: Catalytic activities of toluene and apparent activation energies (Ea) of all catalysts.

Author Contributions: S.J.: Data curation, Software, Writing-original draft. Z.Y.: Conceptualization, Methodology, Writing—review & editing. N.T.: Supervision. All authors have read and agreed to the published version of the manuscript.

Funding: This research received no external funding.

Institutional Review Board Statement: Not applicable.

Informed Consent Statement: Not applicable.

Data Availability Statement: The data presented in this study are available in the article and its supplementary material.

Acknowledgments: We wish to thank College of Environment and Resources, Xiangtan University for providing a congenial work environment and state-of-the-art research facilities. We also thank Zhimin You for his valuable support, comments, and suggestions.

Conflicts of Interest: The authors declare no conflict of interest.

Declaration of Competing Interest: The authors declare that they have no known competing financial interest or personal relationships that could have appeared to influence the work reported in this paper.

References

1. Kamal, M.S.; Razzak, S.A.; Hossain, M.M. Catalytic oxidation of volatile organic compounds (VOCs)–A review. *Atmos. Environ.* **2016**, *140*, 117–134. [CrossRef]
2. Dai, C.; Zhou, Y.; Peng, H.; Huang, S.; Qin, P.; Zhang, J.; Yang, Y.; Luo, L.; Zhang, X. Current progress in remediation of chlorinated volatile organic compounds: A review. *J. Ind. Eng. Chem.* **2018**, *62*, 106–119. [CrossRef]
3. Li, J.; Lu, R.; Dou, B.; Ma, C.; Hu, Q.; Liang, Y.; Wu, F.; Qiao, S.; Hao, Z. Porous Graphitized Carbon for Adsorptive Removal of Benzene and the Electrothermal Regeneration. *Environ. Sci. Technol.* **2012**, *46*, 12648–12654. [CrossRef]
4. Jiang, Z.; Feng, X.; Deng, J.; He, C.; Douthwaite, M.; Yu, Y.; Liu, J.; Hao, Z.; Zhao, Z. Atomic-Scale Insights into the Low-Temperature Oxidation of Methanol over a Single-Atom Pt_1-Co_3O_4 Catalyst. *Adv. Funct. Mater.* **2019**, *29*, 1902041. [CrossRef]
5. Zhang, Q.; Yuan, B.; Shao, M.; Wang, X.; Lu, S.; Lu, K.; Wang, M.; Chen, L.; Chang, C.C.; Liu, S. Variations of ground-level O-3 and its precursors in Beijing in summertime between 2005 and 2011. *Atmos. Chem. Phys.* **2014**, *14*, 6089–6101. [CrossRef]
6. Yang, C.; Miao, G.; Pi, Y.; Xia, Q.; Wu, J.; Li, Z.; Xiao, J. Abatement of various types of VOCs by adsorption/catalytic oxidation: A review. *Chem. Eng. J.* **2019**, *370*, 1128–1153. [CrossRef]
7. Jiang, Z.; He, C.; Dummer, N.F.; Shi, J.; Tian, M.; Ma, C.; Hao, Z.; Taylor, S.H.; Ma, M.; Shen, Z. Insight into the efficient oxidation of methyl-ethyl-ketone over hierarchically micro-mesostructured Pt/K-(Al)SiO_2 nanorod catalysts: Structure-activity relationships and mechanism. *Appl. Catal. B Environ.* **2018**, *226*, 220–233. [CrossRef]
8. Tian, M.; He, C.; Yu, Y.; Pan, H.; Smith, L.; Jiang, Z.; Gao, N.; Jian, Y.; Hao, Z.; Zhu, Q. Catalytic oxidation of 1,2-dichloroethane over three-dimensional ordered meso-macroporous Co_3O_4/$La_{0.7}Sr_{0.3}Fe_{0.5}Co_{0.5}O_3$: Destruction route and mechanism. *Appl. Catal. A Gen.* **2018**, *553*, 1–14. [CrossRef]
9. Zhang, X.; Song, L.; Bi, F.; Zhang, D.; Wang, Y.; Cui, L. Catalytic oxidation of toluene using a facile synthesized Ag nanoparticle supported on UiO-66 derivative. *J. Colloid Interface Sci.* **2020**, *571*, 38–47. [CrossRef] [PubMed]
10. Mo, S.; Zhang, Q.; Li, J.; Sun, Y.; Ren, Q.; Zou, S.; Zhang, Q.; Lu, J.; Fu, M.; Mo, D.; et al. Highly efficient mesoporous MnO_2 catalysts for the total toluene oxidation: Oxygen-Vacancy defect engineering and involved intermediates using in situ DRIFTS. *Appl. Catal. B Environ.* **2020**, *264*, 118464. [CrossRef]
11. He, C.; Cheng, J.; Zhang, X.; Douthwaite, M.; Pattisson, S.; Hao, Z. Recent Advances in the Catalytic Oxidation of Volatile Organic Compounds: A Review Based on Pollutant Sorts and Sources. *Chem. Rev.* **2019**, *119*, 4471–4568. [CrossRef] [PubMed]
12. Fang, Y.; Guo, Y. Copper-based non-precious metal heterogeneous catalysts for environmental remediation. *Chin. J. Catal.* **2018**, *39*, 566–582. [CrossRef]

13. Ren, Q.; Feng, Z.; Mo, S.; Huang, C.; Li, S.; Zhang, W.; Chen, L.; Fu, M.; Wu, J.; Ye, D. 1D-Co_3O_4, 2D-Co_3O_4, 3D-Co_3O_4 for catalytic oxidation of toluene. *Catal. Today* **2019**, *332*, 160–167. [CrossRef]
14. Zhang, Q.; Mo, S.; Chen, B.; Zhang, W.; Huang, C.; Ye, D. Hierarchical Co_3O_4 nanostructures in-situ grown on 3D nickel foam towards toluene oxidation. *Mol. Catal.* **2018**, *454*, 12–20. [CrossRef]
15. Kołodziej, A.; Łojewska, J.; Tyczkowski, J.; Jodłowski, P.; Redzynia, W.; Iwaniszyn, M.; Zapotoczny, S.; Kuśtrowski, P. Coupled engineering and chemical approach to the design of a catalytic structured reactor for combustion of VOCs: Cobalt oxide catalyst on knitted wire gauzes. *Chem. Eng. J.* **2012**, *200–202*, 329–337. [CrossRef]
16. Liu, Q.; Wang, L.-C.; Chen, M.; Cao, Y.; He, H.-Y.; Fan, K.-N. Dry citrate-precursor synthesized nanocrystalline cobalt oxide as highly active catalyst for total oxidation of propane. *J. Catal.* **2009**, *263*, 104–113. [CrossRef]
17. Ren, Q.; Mo, S.; Peng, R.; Feng, Z.; Zhang, M.; Chen, L.; Fu, M.; Wu, J.; Ye, D. Controllable synthesis of 3D hierarchical Co_3O_4 nanocatalysts with various morphologies for the catalytic oxidation of toluene. *J. Mater. Chem. A* **2018**, *6*, 498–509. [CrossRef]
18. Qian, S.; Wang, C.; Liu, W.; Zhu, Y.; Yao, W.; Lu, X. An enhanced CdS/TiO_2 photocatalyst with high stability and activity: Effect of mesoporous substrate and bifunctional linking molecule. *J. Mater. Chem.* **2011**, *21*, 4945–4952. [CrossRef]
19. Liu, B.; Vellingiri, K.; Jo, S.-H.; Kumar, P.; Ok, Y.S.; Kim, K.-H. Recent advances in controlled modification of the size and morphology of metal-organic frameworks. *Nano Res.* **2018**, *11*, 4441–4467. [CrossRef]
20. He, H.; Li, R.; Yang, Z.; Chai, L.; Jin, L.; Alhassan, S.I.; Ren, L.; Wang, H.; Huang, L. Preparation of MOFs and MOFs derived materials and their catalytic application in air pollution: A review. *Catal. Today* **2021**, *375*, 10–29. [CrossRef]
21. Liu, H.; Zhang, S.; Liu, Y.; Yang, Z.; Feng, X.; Lu, X.; Huo, F. Well-Dispersed and Size-Controlled Supported Metal Oxide Nanoparticles Derived from MOF Composites and Further Application in Catalysis. *Small* **2015**, *11*, 3130–3134. [CrossRef] [PubMed]
22. Lei, J.; Wang, S.; Li, J. Mesoporous Co_3O_4 derived from Co-MOFs with different morphologies and ligands for toluene catalytic oxidation. *Chem. Eng. Sci.* **2020**, *220*, 115654. [CrossRef]
23. Sager, T.M.; Porter, D.W.; Robinson, V.A.; Lindsley, W.G.; Schwegler-Berry, D.E.; Castranova, V. Improved method to disperse nanoparticles for in vitro and in vivo investigation of toxicity. *Nanotoxicology* **2007**, *1*, 118–129. [CrossRef]
24. Lei, J.; Wang, S.; Li, J. Mesoporous Co_3O_4 Derived from Facile Calcination of Octahedral Co-MOFs for Toluene Catalytic Oxidation. *Ind. Eng. Chem. Res.* **2020**, *59*, 5583–5590. [CrossRef]
25. Zhang, X.; Lv, X.; Bi, F.; Lu, G.; Wang, Y. Highly efficient Mn_2O_3 catalysts derived from Mn-MOFs for toluene oxidation: The influence of MOFs precursors. *Mol. Catal.* **2020**, *482*, 110701. [CrossRef]
26. Du, Y.; Meng, Q.; Wang, J.; Yan, J.; Fan, H.; Liu, Y.; Dai, H. Three-dimensional mesoporous manganese oxides and cobalt oxides: High-efficiency catalysts for the removal of toluene and carbon monoxide. *Microporous Mesoporous Mater.* **2012**, *162*, 199–206. [CrossRef]
27. Feng, X.; Guo, J.; Wen, X.; Xu, M.; Chu, Y.; Yuan, S. Enhancing performance of Co/CeO_2 catalyst by Sr doping for catalytic combustion of toluene. *Appl. Surf. Sci.* **2018**, *445*, 145–153. [CrossRef]
28. Mo, S.; Li, S.; Li, J.; Deng, Y.; Peng, S.; Chen, J.; Chen, Y. Rich surface Co(iii) ions-enhanced Co nanocatalyst benzene/toluene oxidation performance derived from Co(II)Co(III) layered double hydroxide. *Nanoscale* **2016**, *8*, 15763–15773. [CrossRef]
29. Xu, L.; Jiang, Q.; Xiao, Z.; Li, X.; Huo, J.; Wang, S.; Dai, L. Plasma-Engraved Co_3 O_4 Nanosheets with Oxygen Vacancies and High Surface Area for the Oxygen Evolution Reaction. *Angew. Chem.* **2016**, *55*, 5277–5281. [CrossRef]
30. Wang, X.; Liu, Y.; Zhang, T.; Luo, Y.; Lan, Z.; Zhang, K.; Zuo, J.; Jiang, L.; Wang, R. Geometrical-Site-Dependent Catalytic Activity of Ordered Mesoporous Co-Based Spinel for Benzene Oxidation: In Situ DRIFTS Study Coupled with Raman and XAFS Spectroscopy. *ACS Catal.* **2017**, *7*, 1626–1636. [CrossRef]
31. Mo, S.; Li, S.; Li, W.; Li, J.; Chen, J.; Chen, Y. Excellent low temperature performance for total benzene oxidation over mesoporous CoMnAl composited oxides from hydrotalcites. *J. Mater. Chem. A* **2016**, *4*, 8113–8122. [CrossRef]
32. Todorova, S.; Kadinov, G.; Tenchev, K.; Kalvachev, Y.; Kostov-Kytin, V. Particle size and support effects on the complete benzene oxidation by Co and Co–Pt catalysts. *J. Mater. Sci.* **2007**, *42*, 3315–3320. [CrossRef]
33. Hu, Z.; Liu, X.; Meng, D.; Guo, Y.; Guo, Y.; Lu, G. Effect of Ceria Crystal Plane on the Physicochemical and Catalytic Properties of Pd/Ceria for CO and Propane Oxidation. *ACS Catal.* **2016**, *6*, 2265–2279. [CrossRef]
34. Zhao, S.; Hu, F.; Li, J. Hierarchical Core–Shell Al_2O_3@Pd-CoAlO Microspheres for Low-Temperature Toluene Combustion. *ACS Catal.* **2016**, *6*, 3433–3441. [CrossRef]
35. Li, J.-B.; Jiang, Z.-Q.; Qian, K.; Huang, W.-X. Effect of Calcination Temperature on Surface Oxygen Vacancies and Catalytic Performance Towards CO Oxidation of Co_3O_4 Nanoparticles Supported on SiO_2. *Chin. J. Chem. Phys.* **2012**, *25*, 103–109. [CrossRef]
36. Sun, H.; Liu, Z.; Chen, S.; Quan, X. The role of lattice oxygen on the activity and selectivity of the OMS-2 catalyst for the total oxidation of toluene. *Chem. Eng. J.* **2015**, *270*, 58–65. [CrossRef]
37. Besselmann, S.; Löffler, E.; Muhler, M. On the role of monomeric vanadyl species in toluene adsorption and oxidation on V_2O_5/TiO_2 catalysts: A Raman and in situ DRIFTS study. *J. Mol. Catal. A Chem.* **2000**, *162*, 401–411. [CrossRef]
38. Lei, J.; Wang, S.; Li, J.; Xu, Y.; Li, S. Different effect of Y (Y = Cu, Mn, Fe, Ni) doping on Co_3O_4 derived from Co-MOF for toluene catalytic destruction. *Chem. Eng. Sci.* **2022**, *251*, 117436. [CrossRef]
39. Jia, Z.; Wang, X.; Thevenet, F.; Rousseau, A. Dynamic probing of plasma-catalytic surface processes: Oxidation of toluene on CeO_2. *Plasma Process. Polym.* **2017**, *14*, 1600114. [CrossRef]

40. Araña, J.; González Díaz, O.; Miranda Saracho, M.; Doña Rodríguez, J.M.; Herrera Melián, J.A.; Pérez Peña, J. Photocatalytic degradation of formic acid using Fe/TiO_2 catalysts: The role of Fe^{3+}/Fe^{2+} ions in the degradation mechanism. *Appl. Catal. B Environ.* **2001**, *32*, 49–61. [CrossRef]
41. Chen, X.; Chen, X.; Yu, E.; Cai, S.; Jia, H.; Chen, J.; Liang, P. In situ pyrolysis of Ce-MOF to prepare CeO_2 catalyst with obviously improved catalytic performance for toluene combustion. *Chem. Eng. J.* **2018**, *344*, 469–479. [CrossRef]
42. Du, J.; Qu, Z.; Dong, C.; Song, L.; Qin, Y.; Huang, N. Low-temperature abatement of toluene over Mn-Ce oxides catalysts synthesized by a modified hydrothermal approach. *Appl. Surf. Sci.* **2018**, *433*, 1025–1035. [CrossRef]

Disclaimer/Publisher's Note: The statements, opinions and data contained in all publications are solely those of the individual author(s) and contributor(s) and not of MDPI and/or the editor(s). MDPI and/or the editor(s) disclaim responsibility for any injury to people or property resulting from any ideas, methods, instructions or products referred to in the content.